

Ranger: Boosting Error Resilience of Deep Neural Networks through Range Restriction

Zitao Chen
University of British Columbia
Email: zitaoc@ece.ubc.ca

Guanpeng Li
University of Illinois
Email: guanpeng@illinois.edu

Karthik Pattabiraman
University of British Columbia
Email: karthikp@ece.ubc.ca

Abstract—With the emerging adoption of deep neural networks (DNNs) in the HPC domain, the reliability of DNNs is also growing in importance. As prior studies demonstrate the vulnerability of DNNs to hardware transient faults (i.e., soft errors), there is a compelling need for an efficient technique to protect DNNs from soft errors. While the inherent resilience of DNNs can tolerate some transient faults (which would not affect the system’s output), prior work has found there are *critical faults* that cause safety violations (e.g., misclassification). In this work, we exploit the inherent resilience of DNNs to protect the DNNs from critical faults. In particular, we propose *Ranger*, an automated technique to selectively restrict the ranges of values in particular DNN layers, which can dampen the large deviations typically caused by critical faults to smaller ones. Such reduced deviations can usually be *tolerated* by the inherent resilience of DNNs. *Ranger* can be integrated into existing DNNs without retraining, and with minimal effort. Our evaluation on 8 DNNs (including two used in self-driving car applications) demonstrates that *Ranger* can achieve significant resilience boosting without degrading the accuracy of the model, and incurring negligible overheads.

I. INTRODUCTION

In the recent past, there has been wide adoption of deep neural networks (DNNs) in the High-Performance Computing (HPC) domain [1]–[4]. One of the defining characteristics of DNNs is the humongous data they use, which requires large-scale HPC resources. Typical DNNs are composed of a large number of identical neurons that are highly parallel in nature [5], which maps naturally to parallel processors such as multi-core CPUs, GPUs, or even specialized hardware accelerators (e.g., TPU [6]). These hardware accelerators are mini-supercomputers in their own right. For example, the Nvidia Orin system, which is a DNN accelerator is able to deliver 200 TOPS (trillion operations per second) [7].

As DNNs are deployed on HPC systems, their reliability becomes important [8], [9]. In particular, HPC systems are vulnerable to hardware transient faults (i.e., soft errors), which are growing in frequency due to the increase in system scale (particularly in the HPC domain [10]–[12]). Soft errors typically manifest as bit-flips in the system and can be induced by high-energy particle strikes (e.g., alpha particles), transistor variability, thermal cycling, and malicious attacks [13]. This is important because HPC applications require not only high performance, but also *high fidelity* results. For example, in the health-care domain, DNNs have been trained to extract meaningful information from the large amount of historical

data, and hence assist in precision medical diagnosis (e.g., detection of atrial fibrillation) [3], [14], [15].

Another emerging example are Autonomous Vehicles (AVs), in which DNNs are used to provide end-to-end autonomy. An AV system can be considered as a moving data center that constantly aggregates the sensory data from the surroundings, from which the system needs to provide prompt and reliable results to safely navigate the vehicles. In AVs, hardware transient faults could result in safety violations such as causing the AV system to miss obstacles in its path [16], [17]. Further, many of these applications have to adhere to standards, e.g., the ISO 26262 standard [18] for AVs requires that there should be no more than 10 FIT (Failure in Time), which translates to 10 failures in a billion hours of operation. Therefore, it is important to protect DNN systems from soft errors.

Traditional methods to protect systems from soft errors use redundancy at the hardware level (e.g., Dual-Modular Redundancy). However, such techniques are prohibitively expensive, and are impractical to be used in this domain. For example, the cost-per-unit and computation performance are of significant importance in the HPC domain. Duplicating hardware components adds to the total cost of the system, and requires synchronization and voting. DNN-specific techniques have been proposed to enhance the error resilience of DNNs [16], [19], [20]. However, they either suffer from significant false positives (e.g., raise an alarm when there is no fault present), or require significant implementation effort (Section VI). Therefore, there is a compelling need for an *efficient technique to boost the error resilience of DNNs*.

In this paper, we leverage the inherent resilience of DNNs to enable efficient fault correction to protect them from critical faults, by selectively restricting the values in DNNs. *Critical faults* are those faults that corrupt the outputs of DNNs, e.g., cause mis-classification in classification networks, leading to safety violations. Such failures are also known as Silent Data Corruptions (SDCs). We propose *Ranger*, a technique to selectively restrict the ranges of values in specific DNN layers, thereby reducing the SDCs due to critical faults.

Ranger dampens the large value deviations to small ones, which can be *tolerated* by the inherent resilience of DNNs, i.e., DNNs are still able to generate correct outputs. Note that the values that exceed the restriction bound are not limited to those corrupted by critical faults. For the values that are corrupted by faults, *Ranger* can restrict the ranges of the values to prevent

SDCs. However, for normal values (i.e., those uncorrupted by the fault), range restriction due to *Ranger* will not degrade the accuracy of the original model (Section III-B).

Ranger is an automated transformation applied on existing DNN models. Thus, existing DNN applications can benefit from *Ranger*, without requiring the retraining of the DNNs. This is very important as retraining DNNs can consume significant computational resources, especially for large networks used in the HPC domain. Further, the only effort needed by the programmer to apply *Ranger* is to provide representative inputs for deriving the restriction bounds (e.g., randomly choose 20% of training data in the dataset), which are used for range restriction. Finally, *Ranger* incurs very low performance overheads in practice (Section IV). *Therefore, Ranger is practical to use in DNN applications used in HPC.*

Prior work has used value truncation for different purposes, such as improving the performance of Machine Learning (ML) [5], [21]; increasing the robustness of ML models to outliers [22], and preserving the privacy of ML [23], [24] (Section VI). However, we leverage value restriction for improving the error resilience of ML to transient faults. Our work is inspired by a recent paper by Chen *et al.* [17], which distinguishes between benign faults and critical faults based on the mathematical properties of the ML model to perform efficient fault injection. However, Chen *et al.* do not propose any technique to protect the DNNs from the critical faults. *To the best of our knowledge, Ranger is the first technique to provide efficient fault correction for transient faults in DNNs, without requiring significant effort or retraining.*

The main contributions of this paper are as follows:

- Propose *Ranger*, an automated technique to selectively restrict the ranges of values in DNNs, and transform large values into smaller ones. Thus, large deviations caused by critical faults will be restricted, and can be tolerated by DNNs (due to the inherent resilience of DNNs).
- Present an approach to choose particular layers in DNNs for range restriction by studying their value dependency, as well as derive the restriction bounds to be used by *Ranger*.
- Perform an experimental evaluation of *Ranger* on 8 DNN models with a total of 5 datasets (including two DNN applications in the AV domain). The evaluation demonstrates that *Ranger*: 1) significantly enhances the resilience of the DNNs models - it reduces the SDC rates from 14.92% to 0.44% (in classifier DNNs), and from 23.76% to 2.49% (in the AV DNNs); 2) does not degrade the accuracy of any of the evaluated models, and 3) incurs negligible memory and performance overheads (0.518% on average).

II. BACKGROUND AND FAULT MODEL

A. Deep Learning

Deep learning is a field of artificial intelligence that typically leverages DNNs to address problems in both classification and regression. In this paper, we primarily consider convolutional neural networks (CNNs), a class of DNNs application (others such as recurrent neural networks [5] are not considered). A

typical DNN uses multiple layers to progressively extract high level features from the raw input. The primary computation usually occurs in the convolution (Conv) layer that extracts the underlying patterns. The results are then fed to the activation (ACT) layer in which the ACT function is used to determine how the neuron should be activated (e.g., performing non-linear transformation). Other layers such as pooling, normalization layers can be added following the ACT layer. The layer closest to the output is usually called fully-connected (FC) layer. An DNN model typically goes through 2 phases: 1) training phase in which the model is trained to learn particular task; 2) inference phase where the model is used for actual deployment.

B. Fault Model

In this study, we consider hardware transient faults (i.e., soft errors) that occur randomly during the inference phase of the DNNs. We consider inference phase because DNNs are usually trained once, while the inference task is performed repeatedly in deployment, and are hence much more likely to experience faults during their lifetime, and faults in inference phase can cause damaging consequences (e.g., cause the AVs to miss the obstacles in its path; misclassify the “stop” sign as “yield” sign) [16], [17], [19], [25]. On the other hand, the training process of the DNN is known to be able to overcome small noisy data as it is a statistical learning process [5] - thus faults in the learning phase are unlikely to cause as much damage as in the inference phase. We assume that faults arise in the processor’s data path (ALUs and pipeline registers); and faults in main memory, cache and register file are protected by ECC or parity [26]. This is in line with previous reliability studies [27]–[29]. In addition, we assume that faults do not arise in the control logic of the processor, as that constitutes only a small fraction of the total area of the processor. We only consider activated faults as masked faults do not affect the program’s execution.

In recent work, Oliveira *et al.* find that the neutron-induced transient error rate can be as high as 193 FIT (even if ECC is enabled) on the HPC applications executed on the Knights Corner Xeon Phi components [11]. Such high FIT clearly violates the safety standard such as the ISO 26262 (Section I).

We also assume that atmost one fault occurs per program execution, because soft errors are relatively rare events given the typical inference time of DNNs. This also follows the fault models in prior studies [17], [27], [28], [30], [31]. Finally, we inject single bit flips in the software implementation of the DNN, as a transient fault is often manifested as a single bit flip at the software level [32], and studies have shown that multiple bit-flip errors result in similar fault propagation patterns as single bit-flip errors that cause SDCs [33], [34]. We discuss the multiple bit-flip fault model in Section V-D.

III. METHODOLOGY

To protect the DNNs from transient faults (particularly critical faults), we selectively restrict the ranges of values in different DNNs layers. This technique that we call *Ranger*,

is based on two properties in DNNs: 1) the monotonicity of operators in DNNs applications [17]; 2) the inherent resilience of DNNs to insignificant errors [35].

In this section, we start by discussing how transient faults result in output corruption in DNNs (e.g., misclassification). We then explain how the characteristics of critical faults in DNNs, and the inherent resilience of DNNs can be leveraged to improve the error resilience of DNNs. Finally, we elaborate the design of selective range restriction to enable effective error correction without degrading the model’s accuracy.

A. Fault Propagation in DNNs

Unlike traditional programs in which soft errors can corrupt the outputs by diverting the control flow [27], [36], faults that occur in DNNs are typically numerical deviations (e.g., change of the activation value in the feature map). Even the faults that modify connections between neurons can be modeled as numerical deviations. For example, a fault that causes the DNNs to break the connection between two neurons can be considered as a 0 value passed between them.

The output quality of the DNNs is determined by the numerical output. For classification tasks, the output for the correct label needs to be high, and for the incorrect labels, it needs to be low. For regression tasks, the output needs to be as close to the target variable as possible. Therefore, for a fault to corrupt the output of DNNs, it needs to inflict *as large as possible* deviation at the output.

We provide an example on how a fault could effectively result in a misclassification in an DNN, in Fig. 1. For simplicity, the figure only shows two hidden layers L1 and L2, where the colored nodes denote the activated neurons. The darker nodes are those with larger activation values (e.g., Node 6 has a larger activation value than that of Node 7). Though the fault is propagated through all the subsequent connected neurons, not all of them will result in large deviations - smaller deviations are not highlighted for simplicity (e.g., fault propagating from Node 5 to Node 7 because of the weight connection from Node 5 to Node 7 is small).

In the fault-free execution, the classification result is assumed to be correct, i.e., label A. However, when a fault occurs during the computation (Node 5 in the centering network in Fig. 1), it causes a large deviation in the faulty neuron, and this subsequently results in the output for label B to be higher than that of label A. This fault thus leads to a misclassification, and is hence a critical fault. We consider an SDC as any DNN output that deviates from the correct output of the program, e.g., an image mis-classification.

B. Intuition behind Range Restriction

Monotonicity. Chen *et.al* study the mathematical properties of DNNs, and find that many of the computations in DNNs (e.g., ReLu, SoftMax, multiply-accumulate (MAC)) exhibit the monotone property [17]: *monotonically increasing*: $f(x_i) \geq f(x_j), \forall x_i > x_j$; or *monotonically decreasing*: $f(x_i) \leq f(x_j), \forall x_i > x_j$. For example, assume a fault occurs at the Multiply application in the MAC operation and two

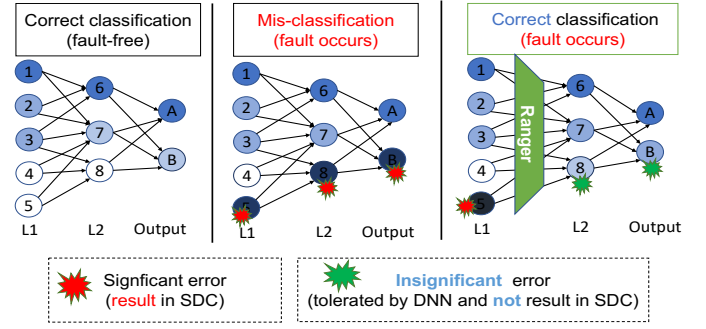


Fig. 1. Example of a fault resulting in misclassification and how *Ranger* enables fault correction by dampening the error to be tolerated by the DNN. Darker colors represent larger activation values. Assume label A is the correct label and B is the incorrect label.

faults x_1, x_2 occur at different bits and x_1 at high-order bit. The monotone property is satisfied as: $|x_1 w_i| \geq |x_2 w_i|$, where w_i is the weight. Therefore, the fault propagation effect caused by x_1 is larger than that by x_2 and thus *more likely* to result in SDC. This property has been found in the common operations (e.g., Convolution, ReLu, etc.) employed in common DNN architectures (e.g., VGGNet, ResNet) by prior work [17].

Thus the fault propagation behavior can be approximated as a monotone function. This monotone property implies that for faults to cause large deviation at the output layer, they should also cause large deviation at the place where they occur. This leads to the observation that critical faults tend to cluster around high-order bits (i.e., causing large value deviation), while faults at low-order bits tend to be masked and not affect the output. Thus range restriction is analogous to “transferring” the faults from high-order bits to low-order bits (since the effect caused by fault is reduced), which can be tolerated by the model itself.

Mitigating critical faults. Typically critical faults in DNNs corrupt the program’s outputs by fault amplification, which would propagate a single fault into multiple values causing large value deviations. Restricting the values in the DNNs reduces the deviations caused by the faults, which in turn lowers the chance of the fault to result in an SDC. This is because DNNs inherently can tolerate small value deviations and generate correct outputs regardless. *Ranger* leverages this property to prevent critical faults from corrupting the outputs, while tolerating other faults. We provide an example in Fig. 1, where the goal of *Ranger* is to reduce the deviation by the critical faults (i.e., significant error) into smaller ones (i.e., insignificant error). Despite the insignificant errors, the system is able to generate the correct output due to the inherent resilience of DNNs.

Maintaining the accuracy of original models. While *Ranger* can be used for fault mitigation, it is also important to ensure that it does not affect the accuracy of the original models. In our evaluation, we derive the restriction bound based on the training data, and evaluate the model on a *separate* validation set, to represent an unbiased approximation for test data, i.e., unseen data. While it is possible that *Ranger*

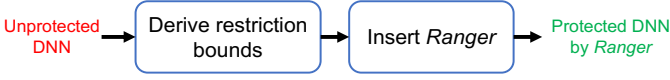


Fig. 2. Work flow of *Ranger*.

might truncate the values during the fault-free execution, this rarely happens as the restriction bound collected from the training data is usually representative of the value ranges (e.g., in the VGG16 model, only in 5 out of 50,000 cases, do the values exceed the restriction bound in the fault-free execution). Moreover, even when the neuronal values in the fault-free execution are restricted (e.g., the 5 cases mentioned above), *Ranger* only truncates the values to the restriction bound. Such value reduction can often be tolerated inherently by the DNNs, and does not lower its accuracy (Section IV-C). Note that we do not require the training data to represent the faulty outcomes (unlike in prior work [19]), and hence we do not need to perform expensive FI experiments to use *Ranger* (though we use FI to evaluate its coverage).

C. Selective Range Restriction

In this section, we explain how to implement *Ranger* in DNNs. The work flow of *Ranger* is shown in Fig. 2. The first step is to *derive the restriction bounds* from the network through profiling, after which we transform the network to *insert Ranger* on selective layers. Finally, the protected DNN with *Ranger* can be released for deployment.

Step 1: Deriving restriction bounds. The restriction bound can be derived from: 1) the function itself, e.g., Tanh function has an inherent bound of $(-1, 1)$: For these functions, we do not have to derive the restriction bounds from the ACT value distribution; 2) Statistical sampling: For functions that are unbounded (such as the ReLu function that does not have an upper bound), the restriction bound can be derived from sampling the distribution of the values in the function, from which we can choose an appropriate bound. Selection of the bound can be adjusted based on whether we are willing to accept accuracy loss for resilience boosting. A conservative approach is to set the bound to the maximal value such that it is less likely to affect the accuracy of the model. Alternatively, we can also choose a smaller bound to gain higher resilience boosting at the cost of accuracy. We choose the conservative approach, but also study the latter approach in our evaluation.

Step 2: Inserting Ranger into selected DNN layers. After deriving the restriction bound, the next step is to apply *Ranger* into the selective layers in DNNs. As mentioned, an DNN typically consists of different layers (e.g., Conv, ACT, Pooling, Normalization, FC, etc). While these different layers can be considered for range restriction, we find that range restriction on the ACT layer is particularly desirable for two reasons: 1) ACT function is used to determine the response from the neuron’s output (e.g., filtering out the negative output in ReLu ACT function), this particular feature of ACT also makes it ideal to be used for “filtering” out the potential critical faults. For example, an ACT function can restrict a large

output from the previous layer (where a transient fault occurs). This restriction thus reduces the deviation caused by faults, lowering the probability of the fault leading to SDCs. 2) ACT function is frequently used in different layers in DNNs (e.g., VGGNet, ResNet, etc), and thus applying range restriction on ACT function effectively dampens fault amplification in between layers (as DNNs usually have many layers).

While range restriction in ACT function would limit the fault amplification effect, it is not sufficient as there are still computations that occur between ACT functions. A single fault in these can quickly propagate and be amplified. We provide an example below to illustrate this problem.

$$y = \text{Relu}_2(\text{Conv}(\text{MaxPool}(\text{ReLu}_1(x)), I)), \quad (1)$$

where ReLu_1 and ReLu_2 are guarded by *Ranger*. Let the bounds of them be $\text{bound}(\text{ReLu}_1) = 10$, $\text{bound}(\text{ReLu}_2) = 1000$. For simplicity, assume $x = [1, 2]$, and $\text{MaxPool}(\text{ReLu}_1(x)) = 2$. Let the Conv layer have n kernels (we assume that each kernel is a simple 1×1 identity kernel I), each of which performs a dot-product computation. Thus the dimension of y is $(n, 1)$.

Assume that a fault occurs at MaxPool function and deviates the MaxPool’s output from 2 to $1024 + 2$. The faulty value of 1026 subsequently propagates through the Conv layer, and thus *all* the elements from y would be affected. In this case, the fault-free output of y is a n -element vector of 2. *Ranger* can restrict the values from 1026 to 1000, thus y becomes a vector of 1000. Such a large value deviation indicates higher probability of resulting in SDCs. And thus applying *Ranger* on the ACT layer alone is *not enough to mitigate critical faults*.

By analyzing the *value dependency* between layers in the model, we find the restriction bound applied to the ACT function can also be *extended* to other functions. Using the same example above, the bound of ReLu_1 is also applicable to the MaxPool function, i.e., $\text{bound}(\text{MaxPool}(\text{ReLu}_1(x))) = \text{bound}(\text{ReLu}_1(x))$. Therefore, the values from MaxPool should not be greater than $\text{bound}(\text{ReLu}_1) = 10$, and thus y will be a vector of 10 even under the the fault in the MaxPool function, which has a significantly lower deviation (compared with a faulty vector with values of 1000). Thus the fault is less likely to cause an SDC as the limited deviation can be tolerated by the inherent resilience of DNNs. Therefore, we need to apply range restriction to selected layers beyond just the ACT function to effectively mitigate SDCs.

We describe the procedure of applying *Ranger* to an unprotected DNN in Algorithm 1. The input to the algorithm is the restriction bounds collected from the profiling process (j pair of upper and lower bounds in total for j ACT layers). The resulting output is the DNN protected with *Ranger*. Line 2 traverses each operation in the network. For each of the ACT operation, the output of it will be bounded (Line 3-4). For all the operations that follow (connect to) the ACT operation and belong to $\{\text{Max-Pool, Avg-Pool, Reshape, Concatenate}\}$, the output of them will also be applied with the *same* restriction

Algorithm 1: Ranger restriction on an unprotected DNN

Input: $i \leftarrow$ number of operation in the model
 $j \leftarrow$ number of ACT operation
 $(low_j, up_j) \leftarrow$ bounds for the j_{th} ACT op

Output: Protected DNN with *Ranger*

```
1: /* Traverse each operation in the network from the first
   layer to the last one */
2: for  $op_i$  in operations in the network do
3:   if  $op_i$  is the  $j_{th}$  ACT operation then
4:     Bound  $op_i$  with  $(low_j, up_j)$ 
5:     if  $op_{i+1}$  in {Max-Pool, Avg-Pool, Reshape} then
6:       Bound  $op_{i+1}$  with  $(low_j, up_j)$ 
7:     else if  $op_{i+1}$  in {Concatenate} then
8:       Bound  $op_{i+1}$  with
          $(\min(low_{j-1}, low_j), \max(up_{j-1}, up_j))$ 
9:     end if
10:  end if
11: end for
12: return Protected DNN
```

bounds (Line 5-8). These are the operations where *Ranger* can be deployed beyond the ACT operation (i.e., the operators protected by *Ranger* remain in the same in the same network). Note that for the Concatenate operation that concatenates the output from the previous 2 ACT operation (this is used in the SqueezeNet model), the restriction bound is derived from the bounds in the preceding 2 ACT operation: lower bound = $\min(low_{j-1}, low_j)$, and upper bound = $\max(up_{j-1}, up_j)$. The time complexity of the algorithm is $O(n)$, where n is the network size.

IV. EVALUATION

A. Software Infrastructure

Implementation of *Ranger*: We have implemented *Ranger* using the TensorFlow framework [37], which is among the most popular framework for writing ML programs today [38]. This allows *Ranger* to be applied to a diverse set of ML programs. In TensorFlow, the program is abstracted as a data-flow graph, which is composed of a set of operators (i.e., different functions). *Ranger* directly modifies the TensorFlow graph by adding the extra operators for range restriction (`tf.math.minimize` and `tf.math.maximize`), as per Algorithm 1 after deriving the restriction bounds.

Note that *Ranger* can also be applied to DNNs written in other ML frameworks such as PyTorch. This is because *Ranger* leverages the inherent properties of the DNN model (e.g., the monotone property of the DNN components, the inherent resilience of DNN), which are platform-independent.

Fault injection tool. We use TensorFI¹, an open-source FI tool for TensorFlow-based programs that allows faults to be injected directly into the TensorFlow graph [39]. We show an example of TensorFI's operation in Fig. 3. The main idea of TensorFI is to duplicate the TensorFlow graph using a set of *customized* operators to perform the fault injection so as

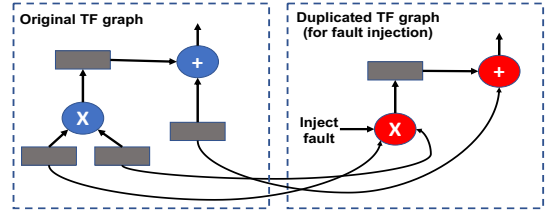


Fig. 3. Example of TensorFlow graph and how a fault is injected into the graph by TensorFI. A fault is injected by duplicating the TensorFlow graph, in which the customized operators support fault injection capability. The nodes in blue represent the original nodes in the graph, while the nodes in red are those added by TensorFI for fault injection [39].

not to interfere with the original graph. As the details of the operations are abstracted from the program in TensorFlow, and are also platform-specific, we inject faults directly to the output values of operators in the graph - this is in line with the FI performed in prior work [16], [17], [19], [39].

B. Experimental Setup

Hardware: Our experiments were conducted on the following machines: 1) an Ubuntu Linux 18.04.2 system with, 8 RTX 2080Ti GPUs, 24 CPUs with 256 GB memory; 2) a Fedora Linux 20 system, 2 GTX TITAN GPUs, 16 CPUs with 256 GB memory; 3) an Ubuntu Linux 16.04 system with 6 CPUs, 1 GeForce GT610 GPU with 16 GB memory.

Research Questions: We evaluate *Ranger* by asking four research questions:

RQ1: What is the effectiveness of *Ranger* in boosting the resilience of DNNs in terms of reducing the SDC rates?

RQ2: Does *Ranger* affect the accuracy of the model?

RQ3: What is the overhead associated with *Ranger*?

RQ4: Is *Ranger* effective in DNNs with reduced precision data types?

DNN benchmarks and datasets. In our evaluation, we evaluate DNNs applications in both classification and regression tasks. In particular, we evaluate 8 different DNNs comprising of common DNN benchmarks in ML studies such as VGGNet, SqueezeNet, ResNet. For the DNNs in regression tasks (where the output is a variable value instead of a class label), we choose two DNNs applications that can be used in the AV domain - these are the applications that can predict the steering angles of the AV. We choose the Nvidia Dave driving model [40] and the steering model from Comma.ai [41]. These DNNs applications have been adopted in real-world vehicles [42] and are thus used as benchmarks for AV studies [17], [43].

We use standard ML datasets (such as MNist, Cifar-10, ImageNet) as well as a real-world driving dataset collected from the images captured by a real vehicle [44]. *MNist* is a popular ML dataset consisting of 60000 images of digits with 10 classes. *Cifar-10* dataset contains 60000 32*32 color images in 10 different classes. *GTSRB* is a dataset collected from the real-world traffic sign for classification and it has 43 different classes of traffic signs. *ImageNet* is a large database

TABLE I
DNN MODELS AND DATASETS USED FOR EVALUATION

DNN model	Dataset	Dataset Description
LeNet	MNist	Hand-written digits
AlexNet	Cifar-10	General images
VGG11	GTSRB	Real-world traffic sign
VGG16	ImageNet	General images
ResNet-18	ImageNet	General images
SqueezeNet	ImageNet	General images
Nvidia Dave [46]	Driving	Real-world driving frames
Comma.ai [41]	Driving	Real-world driving frames

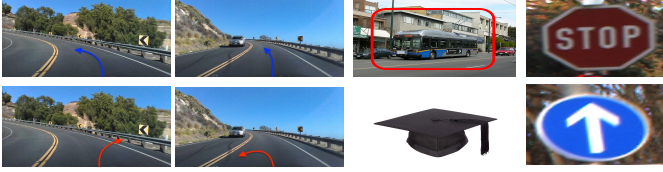


Fig. 4. Example of SDCs in different DNNs in our evaluation. The first row gives the input to the DNN, and the second row shows the output by the DNN due to transient faults.

with more than 14 million images categorized into 1000 different classes.

Table I summarizes the models and datasets in our evaluation. For models using the ImageNet dataset, we report the top-1 accuracy (i.e., the target label is the predicted class that has the highest probability) and the top-5 accuracy (i.e., the target label is one of the top 5 predictions) [16]. For the two steering models, we use RMSE (root mean square error) and the average deviation per frame to evaluate the model’s accuracy - these are used in AV DNN studies [45].

Note that FI experiments on DNNs are highly time-consuming - for each input, we need to perform thousands of FI experiments to obtain a statistically significant estimate of the SDC rate. To limit the experimental time, we choose 10 inputs per model, and ensure the DNNs are able to generate correct prediction on these inputs. We perform 5000 FI trials for each DNN, except for the DNNs using ImageNet, where we perform 3000 FI trials as they are more time-consuming (we verified that the results are statistically significant). We also calculate error bars at the 95% confidence interval.

In our evaluations, we use 32-bit fixed-point data type for the first 3 RQs (this is more energy-efficient than floating-point data type [47]). For RQ4, we evaluate *Ranger* on DNNs using a 16-bit fixed-point data type.

Deriving Restriction Bounds. In our work, we derive the restriction bounds from a randomly-sampled subset of the *training set*. We choose 20% of the training data from each dataset. We find that this is sufficient to derive the ranges for all the DNNs used in our study. For example, Fig. 5 shows the ranges of activation values obtained when sampling different amounts of training data on the VGG16 model. The values

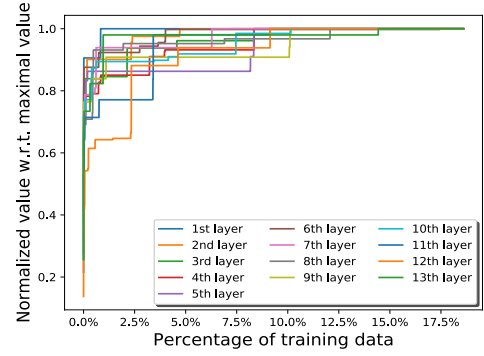


Fig. 5. Range of value observed in each ACT layer using different amount of data on the VGG16 network (13 ACT layers in total). A total of 186056 images (around 20% of the whole training set) were used.

are normalized with respect to the global maximal values (i.e., maximal values on all the sampling data). As shown, the value range quickly converges to the global maximal values for all layers. We observe similar trends in the other networks. This suggests that the range of values collected from the sampling is sufficient to characterize the range of values in the model.

Note that deriving restriction bounds is a one-time cost, and is *incurred before the deployment of the DNN*. In our experiments, it took around one hour to complete this process on the largest network (VGG16) in our evaluation with around 20% of training data in the ImageNet dataset.

To reduce *Ranger*’s effect on the model’s accuracy, we conservatively choose the maximal value observed during the sampling process as the restriction bound (we study the effect of choosing other restriction bounds in Section V).

C. Results

RQ1: Effectiveness of range restriction. We measure the *SDC rate*, which is the percentage of the transient faults that cause SDCs, with and without *Ranger*. For classifier models, an SDC can manifest as an image misclassification. For the two steering models that produce continuous values as outputs, we use different threshold values for the deviations of steering angles to identify SDCs, namely 15, 30, 60 and 120 degrees as done by prior work [17]. Fig. 4 illustrates the effect of SDCs in different DNNs tasks from our experiments.

Note that we only consider those faults that would not lead to obvious system failures such as a crash (e.g., modifying the dimension of a tensor might cause an error, and terminate the program). Though *Ranger* selectively applies range restriction on a subset of operations, we consider faults that can arise randomly in *all* the operations during the computations except the last FC layer. We exclude the last FC layer because values in this layer are directly associated with the final outputs. Thus, restricting the values in the last FC layer is not effective in mitigating SDCs (we validated this in our experiments). However, the state space of the last FC layer constitutes a very small fraction of the state space (e.g., in VGG16 model, the last FC layer only accounts for 0.0047% of the state space),

¹<https://github.com/DependableSystemsLab/TensorFI>

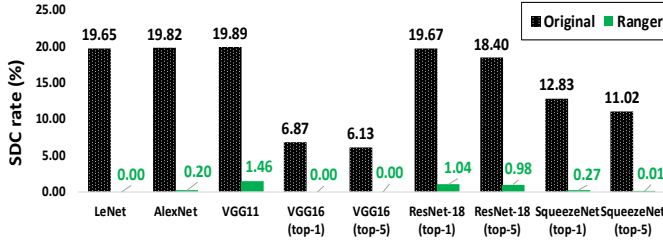


Fig. 6. SDC rates of the original classifier models and enhanced models with *Ranger*. For the models using ImageNet dataset, we provide the results from top-1 and top-5 accuracy. Error bars range from $\pm 0.04\%$ to $\pm 1.46\%$ at the 95% confidence interval. Lower is better.

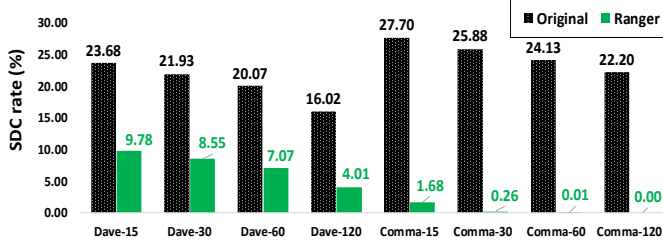


Fig. 7. SDC rates of the original steering models and enhanced models with *Ranger*. SDC is defined by thresholding different degrees of deviation to the correct steering angles (i.e., 15, 30, 60, and 120 degrees). Error bars range from $\pm 0.03\%$ to $\pm 1.24\%$ at the 95% confidence interval. Lower is better.

and techniques such as duplication can be used to protect this particular layer with minimal overheads.

Fig. 6 illustrates the SDC rates in the 6 classifier models with and without *Ranger*. While different DNNs exhibit different SDC rates, Fig. 6 shows that *Ranger* achieves significant SDC reduction across all the models. For example, in the LeNet model, the SDC rate decreases from around 20% to 0% (in our experiments). On average, the SDC rates are reduced from 14.92% to 0.44% across the models.

The results from the two steering models are shown in Fig. 7. In the Comma steering model, *Ranger* can reduce almost all the deviations of steering angles due to transient faults and eliminate large deviations (e.g., 0% of SDCs in the category of threshold=120). However, *Ranger* achieves less pronounced SDC reduction in the Dave model. This is because the Dave model outputs the steering angle in radians, while the Comma model outputs the steering angle in degrees. The conversion from degrees to radians is more sensitive to deviations. This is because the conversion function (Atan function in TensorFlow) is horizontal asymptote ($y \in (-\pi/2, \pi/2)$), and thus even a small deviation at the input of Atan function would cause a large output deviation, i.e., higher SDC probability. Based on this observation, we train a new model which outputs the steering angle in degrees instead of radians, which achieves both *better accuracy and better resilience* with *Ranger* (Section V).

Quantitative Comparison with related work. Hong *et.al* [13] suggest a defense mechanism against memory bit-flips by modifying the ACT functions of the models such as changing

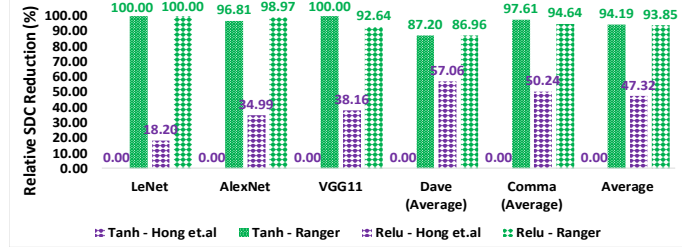


Fig. 8. Relative SDC rate reduction in DNNs following the approach in Hong *et.al* [13] and *Ranger*. Error bars range from $\pm 0.12\%$ to $\pm 1.38\%$ at the 95% confidence interval. Higher is better.

ReLU into Tanh (a similar approach is also proposed in [48]). We compare *Ranger* with the method in Hong *et.al* for 5 of the 8 DNNs. The models we consider are: LeNet, AlexNet, VGG11, Dave and Comma steering model. We only consider 5 models as we need to train a new model for each DNN, and it is time consuming to do so for the other 3 DNNs.

For both approaches, we report the SDC rate reduction relative to the original SDC rates in Fig. 8 (for brevity, we report the average results for the steering models across all the thresholds). Fig. 8 shows that the approach from Hong *et.al* achieves 0% relative SDC reduction in models using Tanh function. This is because transient faults could occur after the Tanh function in the network, and are not affected by the replacement. In contrast, *Ranger* achieves significant SDC reduction because it performs selective range restriction in the entire DNN. For models using the ReLu function, while both approaches can reduce SDC rates, *Ranger* enables significantly higher resilience boosting. For example, for the category of threshold=120 in the two steering models, the SDC rates in Hong *et.al* vary from 4.76% to 9.48%, while with *Ranger* the SDC rates vary from 0% to 0.27%, which is an order of magnitude lower. On average, *Ranger* achieves *more than 90% SDC rate reduction than Hong et.al* across all the models.

Ranger reduces the SDC rate from 14.92% to 0.44% (34X reduction) for the 6 classifier DNNs, from 24.98% to 0.49% on the Comma.ai model (50X reduction), and 20.42% to 7.35% (2.77X reduction) on the Dave model.

RQ2: Accuracy. While Fig. 6 and Fig. 7 demonstrate the effectiveness of *Ranger* in reducing the SDC rates in DNNs, it is also important to understand whether it affects the model's accuracy. Thus, we compare the accuracy of the original models with and without *Ranger*. As mentioned, the restriction bound is derived from sampling the ACT values from a subset of the *training set*. The models are then evaluated on a separate *validation set* (e.g., ImageNet validation set that has 50000 images). We report the accuracy of all the DNNs in Table II.

Our results show that applying *Ranger* does not degrade the accuracy of the baseline models in any of the 8 DNNs. This is because the restriction bounds derived from existing data are sufficient to characterize the ranges of values in the

TABLE II

ACCURACY OF THE ORIGINAL DNN AND THE DNN PROTECTED WITH *Ranger*. + INDICATES ACCURACY IMPROVEMENT. HIGHER IS BETTER.

DNN model	w/o <i>Ranger</i>	w/ <i>Ranger</i>	Diff.
LeNet	99.20%	99.20%	0.00%
AlexNet	82.14%	82.14%	0.00%
VGG11	99.74%	99.74%	0.00%
VGG16 (top-1)	64.72%	64.72%	0.00%
VGG16 (top-5)	85.736%	85.736%	0.00%
ResNet-18 (top-1)	62.66%	62.66%	0.00%
ResNet-18 (top-5)	84.61%	84.61%	0.00%
SqueezeNet (top-1)	52.936%	52.940%	+0.004%
SqueezeNet (top-5)	74.150%	74.154%	+0.004%
Dave (RMSE)	9.808	9.808	0.000
Dave (Avg. Dev.)	3.153	3.153	0.000
Comma (RMSE)	24.122	24.122	0.000
Comma (Avg. Dev.)	12.640	12.640	0.000

DNN. For the rare cases where the normal values exceed the restriction bounds, the value reduction due to *Ranger* does not affect the accuracy. In fact, in the SqueezeNet model, applying range restriction marginally increases the accuracy of the model. This is because the large value corresponding to the incorrect label is reduced by *Ranger*, and thus the classification probability of the incorrect label also decreases.

Ranger does not degrade the accuracy of any of the evaluated DNN models in our experiments.

RQ3: Overhead. We evaluate the runtime overhead of *Ranger* in terms of its memory and performance overhead during the inference phase. The memory overhead comes from the storage for the restriction bounds, which is proportional to the number of ACT functions in the models (the restriction bounds are applicable for not just ACT functions, but also others such as MaxPool function). Given the typical size of the DNNs, this memory overhead is negligible (e.g., VGG16 model has a size of over 500MB).

We first measure the absolute runtime of the DNN models. The average inference time across all the models (using GPUs) is 9.41 milliseconds (without *Ranger*) and 9.64 milliseconds (with *Ranger*), with $\pm 0.11\%$ standard deviation. Note that the absolute runtime is highly dependent on the hardware architecture and system configuration. Therefore, for reproducibility purposes, we measure the performance overhead of *Ranger* in terms of the floating-point operations (FLOPs) incurred by it. FLOPs is a measure of the latency and energy consumption of ML models [49]–[51], and is independent of the hardware platform. We use the TensorFlow profiler for this purpose.

The results are reported in Table III. We did not observe variations across different inputs as they all have the same dimension. We find that the overhead of *Ranger* to be very

TABLE III

COMPUTATION OVERHEAD (FLOPS) OF *Ranger*. M STANDS FOR MILLION; B STANDS FOR BILLION.

DNN model	w/o <i>Ranger</i>	w/ <i>Ranger</i>	Overhead
LeNet	24.622M	24.722M	0.408%
AlexNet	11.361M	11.468M	0.937%
VGG11	87.057M	87.326M	0.309%
VGG16	309.604B	309.905B	0.097%
ResNet-18	36.354B	36.404B	0.138%
SqueezeNet	530.813M	539.215M	1.583%
Dave	56.545M	56.764M	0.387%
Comma	17.673M	17.723M	0.282%

low (0.518% on average) - this is negligible in most cases. This is because *Ranger* only involves range checking and truncation, which are relatively simple operations, compared to the typical operators in a DNN. We have only evaluated the overhead of *Ranger* on TensorFlow programs - however, we believe it should be small on other frameworks as well given the simplicity of range restriction.

Ranger incurs negligible performance and memory overheads on average across the DNN models.

RQ4: Effectiveness of *Ranger* under reduced precision data type. In previous RQs, we used a 32-bit fixed-point data type, which is more energy-efficient than a floating-point data type. The data type precision can be reduced to gain further energy efficiency [47]. Therefore, we study the effectiveness of *Ranger* in DNNs using 16-bit fixed-point data type, which can be used for inference in large DNNs (using smaller data types such as 8-bit datatype cannot provide enough dynamic value range for large DNNs [47]). While it is possible to use quantization such that the same 8-bit data width can represent larger value range, this is similar to using standard fixed-point datatypes without quantization (e.g., a quantized 8-bit datatype can represent comparable range as the unquantized 16-bit datatype). We use 14 bits for integer and 2 for fractional part, which is sufficient for most common DNNs [47].

As before, we report the SDC rates of the models with and without *Ranger* in Fig. 9. As shown, *Ranger* is effective in reducing the SDC rate of all 8 DNNs, from 15.11% to 0.93% (a 16X reduction) even with reduced precision data types.

V. DISCUSSION

In this section, we first study the trade off between accuracy and resilience in *Ranger*. We then discuss the design alternatives for *Ranger*, the limitations of our work, and finally the extension of our work to the multiple bit-flip fault model.

A. Trade-off between Accuracy and Resilience.

We study how to adjust the restriction bound to gain additional resilience at the cost of accuracy (e.g., in systems

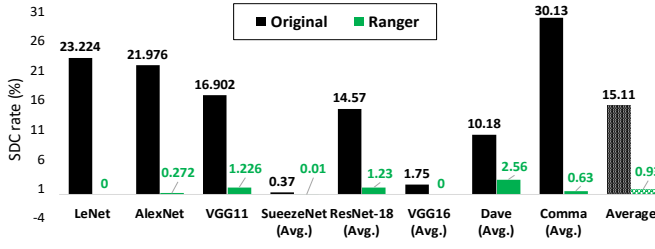


Fig. 9. SDC rate of DNNs using 16-bit fixed-point data type. Error bars range from $\pm 0.04\%$ to $\pm 1.33\%$ at the 95% confidence interval. Lower is better.

that are more prone to transient faults). We focus on the Dave steering model because as shown in Fig. 7, the average SDC rate is around 7% even when protected with *Ranger*.

As mentioned, *Ranger* does not yield significant SDC reduction on the original Dave model that outputs the radian value. Therefore, we train a new Dave model whose output is the steering angle in degrees. We then evaluate both the accuracy and SDC rate of the model using different restriction bound values. As mentioned in Section III, we collect the distribution of ACT values from statistical sampling, and can choose the restriction bound accordingly. For example, setting the restriction bound to the 100th percentile means we use the value that covers *all of the sampled values* (i.e., the maximum value) - this was our earlier approach in Section IV.

Fig. 10 shows the SDC rates of the model with different restriction bound percentiles, and Table IV shows the corresponding accuracy values. As shown, the SDC rate reduction due to *Ranger* is higher than that in Fig. 7, leading to a lower SDC rate with *Ranger*. For example, when applying *Ranger* in both models, the SDC rate for the category of *threshold=120* is 4.01% in the original Dave model, and 2.23% in the new one. *Ranger* does not degrade the accuracy of either model. In addition, the accuracy of the new Dave model is higher than that in Fig. 7. This is because the new model outputs the steering angle in degrees, which has a larger dynamic range than radian values, thereby allowing the model to make more accurate predictions.

As expected, setting a restriction bound to a lower-percentile value boosts the resilience but also degrades the accuracy of the models. When comparing the models using 100% bound and 99.9% bound, the average deviation per frame increases from 2.651 to 2.883. However, this provides a higher resilience boost, e.g., the SDC rate for *threshold=120* reduces from 2.23% to 0.27%. On average, choosing the 99.9% percentile restriction bound reduces the SDC rate from 22.54% to 2.9%, for the Dave model, with only marginal accuracy loss.

B. Design Alternatives for Ranger

Value replacement strategy: While *Ranger* restores out-of-bound values to the restriction bound, we explore other design alternatives for *Ranger* based on other work. For example, Reagan *et al.* propose to reset the faulty value to 0 upon the detection of a fault [52]. Similarly, we can restrict all the out-of-bound value to 0, instead of the restriction bound. We

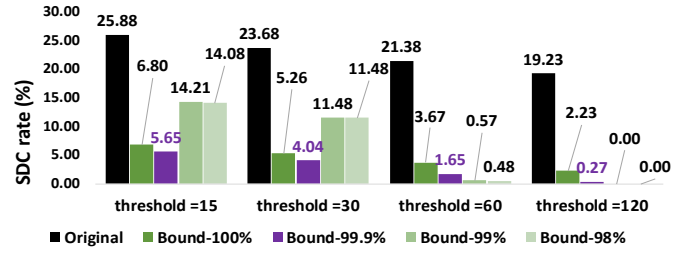


Fig. 10. SDC rates for Dave model Vs. restriction bounds. Error bars range from $\pm 0.14\%$ to $\pm 1.39\%$ at the 95% confidence interval. Lower is better.

TABLE IV
ACCURACY DIFFERENCE OF THE DAVE MODEL WITH DIFFERENT RESTRICTION BOUNDS. LOWER IS BETTER.

Accuracy	Original	100% Bound	99.9% Bound	99% Bound	98% Bound
RMSE	6.069	6.069	8.5719	12.370	13.940
Avg. Deviation	2.651	2.651	2.883	4.077	4.884

conduct a targeted experiment on the VGG16 model using this strategy. We observe that resetting values beyond the bound to 0 significantly degrades the accuracy of the original model (e.g., $3/5=60\%$ of the inputs are inaccurate after the resetting). This is because the value reduction is so drastic that the model is not able to generate a correct output. Further, resetting the values to 0 is likely to cause 0 values in subsequent operations, such as multiplication, which can lead to incorrect results.

Another possible strategy is to replace out-of-bound values with a random value between 0 and the restriction bound. We perform another targeted experiment where we reset values outside the restriction range to random values (within the restriction bound) - we inject 1000 faults for this experiment. Even though some of the classification results change (where the incorrectly predicted labels change), the top-1 and top-5 accuracies remain the same. Therefore, the random replacement strategy is also a viable one, though *Ranger* is much more deterministic and may be preferred for safety-critical systems.

C. Limitations

Despite our results to the contrary, *Ranger* might decrease the model's accuracy in some cases, because of the insufficiency of the data to characterize the unseen data in the real world. However, there is no easy remedy for this problem and using a validation set (as per our evaluation) is a common practice to evaluate the generalizability of the trained models (in our case, the models are the ones applied with *Ranger*). For the rare cases where the normal values exceed the restriction bound, *Ranger* still does not degrade the accuracy of the model (based on our evaluation). Therefore, even if there is an accuracy degradation in the DNNs due to *Ranger* in real-world scenarios, such degradation is unlikely to be high due to the inherent resilience to insignificant errors in DNNs.

While *Ranger* enables significant resilience boosting in different DNNs, even to 0% in some models (e.g., LeNet, VGG16), we can still observe a small margin of SDCs in some of the models. This indicates that DNNs systems are still vulnerable to a small number of critical faults. We attribute this to the heterogeneous patterns of the critical faults in different DNNs. In particular, while most critical faults need to result in large deviations to cause SDCs, this is not always the case. We can reduce the restriction bound to gain further SDC reduction at the cost of accuracy as we have shown above.

With the above said, transient faults are relatively rare events, and *Ranger* only leaves unprotected 0.44% of SDCs in 6 of the classifier DNNs and 2.49% in the two steering models (using degrees in the Dave model). Further, it does not degrade the accuracy of the original model, incurs negligible performance overheads, and requires no retraining. Therefore, we believe it is practical in real-world HPC systems.

D. Discussion for multiple bit-flips scenario

In this section, we discuss the effectiveness of *Ranger* under the presence of multi-bit flips. Multi-bit flips will potentially result in *more* values being affected than in the single-bit flip case. However, *Ranger* will continue to be effective as it is agnostic to the number of out-of-bound values. This is because it restricts *all* the values that exceed the restriction bound.

To validate this, we conducted experiments on two of the classifier models (LeNet and ResNet) and the two DNNs used in AVs. We inject multiple-bit flips (ranging from 2 bits to 5 bits) at randomly chosen values. These multi-bit faults can affect *multiple* data values - thus they are more potentially damaging as more values will be corrupted by faults. As before, we randomly inject 3000 faults per input per model.

The results are shown in Fig.11 and Fig.12. As can be seen, the SDC rates of the original models increase with the increase of multi-bit flips without *Ranger*. However, with *Ranger*, the SDC rates are significantly lower, in all cases. While the SDC rates for the classifier models protected by *Ranger* remain relatively constant with the number of bit-flips, the SDC rates in the AV DNNs increase with the number of bit flips (although at a slower rate). This is because these DNNs output the steering angle value, which require exactness (unlike classifier model that predicts the classification label). Overall, with multiple bit-flips, the average SDC rate is reduced from 47.55% to 0.87% (55X reduction) for the classifier DNNs; and from 58.38% to 6.97% (8.4X reduction) for the AV DNNs.

VI. RELATED WORK

Assessing the error resilience of a system is often the first step towards protecting it. Therefore, there has been a plethora of work aiming to understand the error resilience of DNNs via fault injection. Li *et al.* assess the resilience of the DNNs by randomly injecting transient faults into the DNN accelerator [16]. This helps identifying the system's resilience under different system design such as the different layers, datatypes. Reagen *et al.* build a fault injection tool to inject faults into the DNNs systems to study the trade

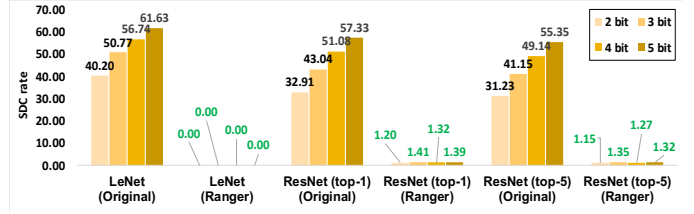


Fig. 11. SDC rates for classifier models (with and without *Ranger*) under multi-bit flips. Numbers denoted in green represent the SDC rates of the models protected by *Ranger*. Error bars range from $\pm 0.38\%$ to $\pm 1.79\%$ at the 95% confidence interval. Lower is better.

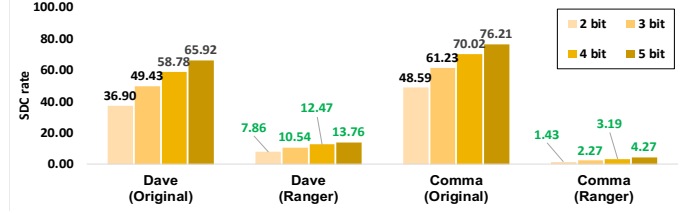


Fig. 12. SDC rates for self-driving models (with and without *Ranger*) under multi-bit flips. Numbers denoted in green represent the SDC rates of the models protected by *Ranger*. Error bars range from $\pm 0.43\%$ to $\pm 1.79\%$ at the 95% confidence interval. Lower is better.

off between model accuracy and fault rate [25]. Santos *et al.* study the resilience of ML application under mixed-precision architectures [53]. Chen *et al.* analyze common ML applications in DNN applications, and identify the monotone property that constrains the fault propagation behavior in ML applications [17]. They identify the unique characteristics of the critical faults in ML applications, which *Ranger* builds on.

Several techniques have been proposed to enhance the error resilience of DNNs [13], [16], [19], [48], [52]. For example, Li *et al.* [16] leverages the value spikes in the neuronal responses as the symptoms for fault detection. However, this technique has a false-positive rate of over 30% [16], and program re-execution is required upon the detection of a fault. This is not desirable for time-critical systems such as AVs where the systems need to generate real-time predictions, and re-execution might cause delay in response. Similarly, Schorn *et al.* [19] builds a supervised learning model to distinguish between benign and critical faults in DNNs, as well as perform error correction. However, their technique requires extensive fault injection (FI), which is particularly time-consuming for large DNNs. For example, for a single input in the VGG16 model, there could be over 30 million values that can be corrupted by faults. Therefore, performing FIs to obtain a comprehensive training set is prohibitively expensive for large DNNs (such large DNNs are not studied in [19]). Techniques based on Algorithm-based Fault Tolerance (ABFT) have also been proposed for detecting faults in particular layers in DNNs (e.g., Conv layer) [54], [55]. However, it does not account for the faults arising in other areas of the DNN, and the fault propagating into multiple neurons. Ozen *et al.* [56] propose to embed safety checksums into the network by introducing a custom regularization term during training. Unfortunately,

their approach requires retraining, which is not desirable for large networks used in the HPC domain. Mahmoud *et al.* [20] use statistical fault injection to identify vulnerable regions in DNNs, and selectively duplicate the vulnerable computations for protection. However, their approach incurs high computational overheads (due to the use of duplication), and also provides only limited protection coverage. For example, they find that duplication with 30% overhead only achieves 40% \sim 70% of error coverage in most of the models (the best coverage is 90% in the SqueezeNet model). In contrast, *Ranger* mitigates an average of 97% of the critical faults in all the classifier models (achieves a 34X reduction in SDC) with only 0.5% performance overhead, and no accuracy loss.

Many studies have used approximate computing techniques to lower the computation and energy demands for DNNs [35], [47], [57]. Leveraging the resilience of DNNs to inexactness in the computations, these studies propose to identify those neurons that have low impact on the final output. They then either replace them with an approximate low-precision design [35] or even remove them altogether [57]. While our study also exploits the inherent resilience of DNNs, we restrict the ranges of values in selected DNN layers rather than find sensitive neurons in the DNNs like prior studies. Further, our goal is not to lower the energy consumption or execution time of the DNN, but to boost its error resilience.

As mentioned earlier, value truncation has been widely used in the ML domain for various purposes (e.g., performance [5], [21]; robustness to outliers [22]; privacy [23], [24]). Gradient clipping is used to address gradient explosion during the training of DNN by rescaling the gradients to a certain range [5]. This is because exploding gradient could result in an unstable network and limiting the magnitude of the gradient can resolve this problem [5]. Truncated gradient is also used to induce sparsity in the learned weights of the online learning algorithm [21]. In addition, the loss function of the model can also be applied with truncation to improve the robustness of the learning algorithm [22]. Value truncation can also be applied to enable privacy preserving ML in the input space during the pre-processing step [23] or to the gradient values [24] (usually along with adding some random noise).

Unlike the above papers, we use range restriction for protecting against transient faults, based on the observation that abnormally large intermediate values in the hidden layers often indicate potential output corruption due to transient faults. In particular, we exploit the *inherent resilience* of DNNs to mitigate critical faults while also maintaining the accuracy of the original model, and leveraging the value dependency between layers for *selective* range restriction.

VII. CONCLUSION

In this work, we propose an efficient resilience boosting technique for DNN applications used in HPC. We present *Ranger*, an automated technique that selectively restricts the ranges of values in DNNs, in order to dampen the large deviations typically caused by critical faults leading to Silent Data Corruptions (SDCs). The reduced deviations can thus be

tolerated by the inherent resilience of DNNs, without causing SDCs. *Ranger* can be easily integrated into existing DNNs.

We evaluate *Ranger* on 8 popular DNN models, 6 of which are classifiers, and two are steering models used in the AV domain. Our evaluation demonstrates that *Ranger* can reduce the SDC rates of the classifier DNNs from 14.92% to 0.44%, and those of the steering models from 23.76% to 2.49%, without degrading the accuracy of the original models, and incurring negligible memory and computation overheads.

REFERENCES

- [1] D. A. Reed and J. Dongarra, "Exascale computing and big data," *Communications of the ACM*, vol. 58, no. 7, pp. 56–68, 2015.
- [2] K. Hazelwood, S. Bird, D. Brooks, S. Chintala, U. Diril, D. Dzhulgakov, M. Fawzy, B. Jia, Y. Jia, A. Kalro *et al.*, "Applied machine learning at facebook: a datacenter infrastructure perspective," in *2018 IEEE International Symposium on High Performance Computer Architecture (HPCA)*. IEEE, 2018, pp. 620–629.
- [3] H.-J. Yoon, A. Ramanathan, and G. Tourassi, "Multi-task deep neural networks for automated extraction of primary site and laterality information from cancer pathology reports," in *INNS Conference on Big Data*. Springer, 2016, pp. 195–204.
- [4] M. Monterrubio-Velasco, J. C. Carrasco-Jimenez, O. Castillo-Reyes, F. Cucchiatti, and J. De la Puente, "A machine learning approach for parameter screening in earthquake simulation," in *2018 30th International Symposium on Computer Architecture and High Performance Computing (SBAC-PAD)*. IEEE, 2018, pp. 348–355.
- [5] I. Goodfellow *et al.*, *Deep learning*. MIT press, 2016.
- [6] "Google tpu." [Online]. Available: <https://cloud.google.com/tpu>
- [7] "Nvidia drive agx." [Online]. Available: <https://www.nvidia.com/en-us/self-driving-cars/drive-platform/hardware/>
- [8] N. DeBardeleben, J. Laros, J. T. Daly, S. L. Scott, C. Engelmann, and B. Harrod, "High-end computing resilience: Analysis of issues facing the hpc community and path-forward for research and development," *Whitepaper*, Dec, 2009.
- [9] B. Schroeder and G. A. Gibson, "Understanding failures in petascale computers," in *Journal of Physics: Conference Series*, vol. 78, no. 1. IOP Publishing, 2007, p. 012022.
- [10] M. Snir, R. W. Wisniewski, J. A. Abraham, S. V. Adve, S. Bagchi, P. Balaji, J. Belak, P. Bose, F. Cappello, B. Carlson *et al.*, "Addressing failures in exascale computing," *The International Journal of High Performance Computing Applications*, vol. 28, no. 2, pp. 129–173, 2014.
- [11] D. Oliveira, L. Pilla, N. DeBardeleben, S. Blanchard, H. Quinn, I. Koren, P. Navaux, and P. Rech, "Experimental and analytical study of xeon phi reliability," in *Proceedings of the International Conference for High Performance Computing, Networking, Storage and Analysis*, 2017, pp. 1–12.
- [12] L. B. Gomez, F. Cappello, L. Carro, N. DeBardeleben, B. Fang, S. Gurumurthi, K. Pattabiraman, P. Rech, and M. S. Reorda, "Gpgpus: how to combine high computational power with high reliability," in *2014 Design, Automation & Test in Europe Conference & Exhibition (DATE)*. IEEE, 2014, pp. 1–9.
- [13] S. Hong, P. Frigo, Y. Kaya, C. Giuffrida, and T. Dumitras, "Terminal brain damage: Exposing the graceless degradation in deep neural networks under hardware fault attacks," *arXiv preprint arXiv:1906.01017*, 2019.
- [14] Z. Xiong, M. K. Stiles, and J. Zhao, "Robust ecg signal classification for detection of atrial fibrillation using a novel neural network," in *2017 Computing in Cardiology (CinC)*. IEEE, 2017, pp. 1–4.
- [15] P. Rajpurkar, A. Y. Hannun, M. Haghighpanahi, C. Bourn, and A. Y. Ng, "Cardiologist-level arrhythmia detection with convolutional neural networks," *arXiv preprint arXiv:1707.01836*, 2017.
- [16] G. Li, S. K. S. Hari, M. Sullivan, T. Tsai, K. Pattabiraman, J. Emer, and S. W. Keckler, "Understanding error propagation in deep learning neural network (dnn) accelerators and applications," in *Proceedings of the International Conference for High Performance Computing, Networking, Storage and Analysis*. ACM, 2017, p. 8.
- [17] Z. Chen *et al.*, "Binfi: An efficient fault injector for safety-critical machine learning systems," in *Proceedings of the International Conference for High Performance Computing, Networking, Storage and Analysis*. ACM, 2019.

- [18] "Functional safety methodologies for automotive applications." [Online]. Available: https://www.cadence.com/content/dam/cadence-www/global/en_US/documents/solutions/automotive-functional-safety-wp.pdf
- [19] C. Schorn *et al.*, "Efficient on-line error detection and mitigation for deep neural network accelerators," in *International Conference on Computer Safety, Reliability, and Security*. Springer, 2018.
- [20] A. Mahmoud, S. K. S. Hari, C. W. Fletcher, S. V. Adve, C. Sakr, N. Shanbhag, P. Molchanov, M. B. Sullivan, T. Tsai, and S. W. Keckler, "Hardnn: Feature map vulnerability evaluation in cnns," *arXiv preprint arXiv:2002.09786*, 2020.
- [21] J. Langford, L. Li, and T. Zhang, "Sparse online learning via truncated gradient," *Journal of Machine Learning Research*, vol. 10, no. Mar, pp. 777–801, 2009.
- [22] Y. Wu and Y. Liu, "Robust truncated hinge loss support vector machines," *Journal of the American Statistical Association*, vol. 102, no. 479, pp. 974–983, 2007.
- [23] Z. Ji, Z. C. Lipton, and C. Elkan, "Differential privacy and machine learning: a survey and review," *arXiv preprint arXiv:1412.7584*, 2014.
- [24] R. Shokri and V. Shmatikov, "Privacy-preserving deep learning," in *Proceedings of the 22nd ACM SIGSAC conference on computer and communications security*, 2015, pp. 1310–1321.
- [25] B. Reagen, U. Gupta, L. Pentecost, P. Whatmough, S. K. Lee, N. Mulholland, D. Brooks, and G.-Y. Wei, "Ares: A framework for quantifying the resilience of deep neural networks," in *2018 55th ACM/ESDA/IEEE Design Automation Conference (DAC)*. IEEE, 2018, pp. 1–6.
- [26] H. Guan *et al.*, "In-place zero-space memory protection for cnn," in *Advances in Neural Information Processing Systems* 32, 2019.
- [27] G. Li, K. Pattabiraman, S. K. S. Hari, M. Sullivan, and T. Tsai, "Modeling soft-error propagation in programs," in *2018 48th Annual IEEE/IFIP International Conference on Dependable Systems and Networks (DSN)*. IEEE, 2018, pp. 27–38.
- [28] R. A. Ashraf, R. Gioiosa, G. Kestor, R. F. DeMara, C.-Y. Cher, and P. Bose, "Understanding the propagation of transient errors in hpc applications," in *SC'15: Proceedings of the International Conference for High Performance Computing, Networking, Storage and Analysis*. IEEE, 2015, pp. 1–12.
- [29] G. Georgakoudis, I. Laguna, D. S. Nikolopoulos, and M. Schulz, "Refine: Realistic fault injection via compiler-based instrumentation for accuracy, portability and speed," in *Proceedings of the International Conference for High Performance Computing, Networking, Storage and Analysis*. ACM, 2017, p. 29.
- [30] B. Fang, K. Pattabiraman, M. Ripeanu, and S. Gurumurthi, "Gpu-qin: A methodology for evaluating the error resilience of gpgpu applications," in *2014 IEEE International Symposium on Performance Analysis of Systems and Software (ISPASS)*. IEEE, 2014, pp. 221–230.
- [31] J. Wei, A. Thomas, G. Li, and K. Pattabiraman, "Quantifying the accuracy of high-level fault injection techniques for hardware faults," in *2014 44th Annual IEEE/IFIP International Conference on Dependable Systems and Networks*. IEEE, 2014, pp. 375–382.
- [32] C.-K. Chang, S. Lym, N. Kelly, M. B. Sullivan, and M. Erez, "Evaluating and accelerating high-fidelity error injection for hpc," in *Proceedings of the International Conference for High Performance Computing, Networking, Storage, and Analysis*, ser. SC '18, 2018, pp. 45:1–45:13.
- [33] B. Sangchoolie, K. Pattabiraman, and J. Karlsson, "One bit is (not) enough: An empirical study of the impact of single and multiple bit-flip errors," in *2017 47th Annual IEEE/IFIP International Conference on Dependable Systems and Networks (DSN)*. IEEE, 2017, pp. 97–108.
- [34] C.-K. Chang, S. Lym, N. Kelly, M. B. Sullivan, and M. Erez, "Evaluating and accelerating high-fidelity error injection for hpc," in *Proceedings of the International Conference for High Performance Computing, Networking, Storage, and Analysis*. IEEE Press, 2018, p. 45.
- [35] S. Venkataramani *et al.*, "Axnn: energy-efficient neuromorphic systems using approximate computing," in *Proceedings of the 2014 international symposium on Low power electronics and design*. ACM, 2014.
- [36] S. K. S. Hari, S. V. Adve, H. Naeimi, and P. Ramachandran, "Relyzer: Exploiting application-level fault equivalence to analyze application resiliency to transient faults," in *ACM SIGPLAN Notices*, vol. 47, no. 4. ACM, 2012, pp. 123–134.
- [37] M. Abadi, P. Barham, J. Chen, Z. Chen, A. Davis, J. Dean, M. Devin, S. Ghemawat, G. Irving, M. Isard *et al.*, "Tensorflow: A system for large-scale machine learning," in *12th {USENIX} Symposium on Operating Systems Design and Implementation ({OSDI} 16)*, 2016, pp. 265–283.
- [38] "Tensorflow popularity." [Online]. Available: <https://towardsdatascience.com/deep-learning-framework-power-scores-2018-23607ddf297a>
- [39] G. Li, K. Pattabiraman, and N. DeBardeleben, "Tensorfi: A configurable fault injector for tensorflow applications," in *2018 IEEE International Symposium on Software Reliability Engineering Workshops (ISSREW)*. IEEE, 2018, pp. 313–320.
- [40] M. Bojarski, D. Del Testa, D. Dworakowski, B. Firner, B. Flepp, P. Goyal, L. D. Jackel, M. Monfort, U. Muller, J. Zhang *et al.*, "End to end learning for self-driving cars," *arXiv preprint arXiv:1604.07316*, 2016.
- [41] "comma.ai's steering model." [Online]. Available: <https://github.com/commaai/research>
- [42] "On-road tests for nvidia dave system." [Online]. Available: <https://devblogs.nvidia.com/deep-learning-self-driving-cars/>
- [43] K. Pei, Y. Cao, J. Yang, and S. Jana, "Deepxplore: Automated whitebox testing of deep learning systems," in *proceedings of the 26th Symposium on Operating Systems Principles*. ACM, 2017, pp. 1–18.
- [44] "Driving dataset." [Online]. Available: <https://github.com/SullyChen/driving-datasets>
- [45] S. Du, *et al.*, "Self-driving car steering angle prediction based on image recognition," *Department of Computer Science, Stanford University, Tech. Rep. CS231-626*, 2017.
- [46] "Tensorflow implementation of nvidia dave system." [Online]. Available: <https://github.com/SullyChen/Autopilot-TensorFlow>
- [47] P. Judd *et al.*, "Proteus: Exploiting precision variability in deep neural networks," *Parallel Computing*, 2018.
- [48] L.-H. Hoang, M. A. Hanif, and M. Shafique, "Ft-clipact: Resilience analysis of deep neural networks and improving their fault tolerance using clipped activation," *arXiv preprint arXiv:1912.00941*, 2019.
- [49] R. Tang, W. Wang, Z. Tu, and J. Lin, "An experimental analysis of the power consumption of convolutional neural networks for keyword spotting," in *2018 IEEE International Conference on Acoustics, Speech and Signal Processing (ICASSP)*. IEEE, 2018, pp. 5479–5483.
- [50] S. Han, J. Pool, J. Tran, and W. Dally, "Learning both weights and connections for efficient neural network," in *Advances in neural information processing systems*, 2015, pp. 1135–1143.
- [51] A. Sehgal and N. Kehtarnavaz, "Guidelines and benchmarks for deployment of deep learning models on smartphones as real-time apps," *Machine Learning and Knowledge Extraction*, vol. 1, no. 1, pp. 450–465, 2019.
- [52] B. Reagen *et al.*, "Minerva: Enabling low-power, highly-accurate deep neural network accelerators," in *ACM/IEEE 43rd Annual International Symposium on Computer Architecture (ISCA)*. IEEE, 2016.
- [53] F. F. dos Santos, C. Lunardi, D. Oliveira, F. Libano, and P. Rech, "Reliability evaluation of mixed-precision architectures," in *2019 IEEE International Symposium on High Performance Computer Architecture (HPCA)*. IEEE, 2019, pp. 238–249.
- [54] K. Zhao, S. Di, S. Li, X. Liang, Y. Zhai, J. Chen, K. Ouyang, F. Cappello, and Z. Chen, "Algorithm-based fault tolerance for convolutional neural networks," *arXiv preprint arXiv:2003.12203*, 2020.
- [55] E. Ozen and A. Orailoglu, "Sanity-check: Boosting the reliability of safety-critical deep neural network applications," in *2019 IEEE 28th Asian Test Symposium (ATS)*. IEEE, 2019, pp. 7–75.
- [56] —, "Concurrent monitoring of operational health in neural networks through balanced output partitions," in *2020 25th Asia and South Pacific Design Automation Conference (ASP-DAC)*. IEEE, 2020, pp. 169–174.
- [57] M. A. Hanif *et al.*, "Error resilience analysis for systematically employing approximate computing in convolutional neural networks," in *2018 Design, Automation & Test in Europe Conference & Exhibition (DATE)*. IEEE, 2018.